JOURNAL OF AIRCRAFT
Vol. 46, No. 1, January–February 2009

National Transonic Facility Model and Tunnel Vibrations

John W. Edwards*
NASA Langley Research Center, Hampton, Virginia 23681-0001

DOI: 10.2514/1.30080

Since coming online in 1984, the National Transonic Facility cryogenic wind tunnel at the NASA Langley Research Center has provided unique high Reynolds number testing capability. Although turbulence levels in the tunnel, expressed in terms of percent of dynamic pressure, are typical of other transonic wind tunnels, the significantly increased load levels used to achieve flight Reynolds numbers, in conjunction with the unique structural design requirements for cryogenic operation, have brought forward the issue of model and model support-structure vibrations. This paper reports computational results and experimental measurements documenting aerodynamic and structural dynamics processes involved in such vibrations experienced in the National Transonic Facility. In particular, evidence of local unsteady airloads developed about the model support strut is shown and related to well-documented acoustic features known as Parker modes. Two-dimensional unsteady viscous computations illustrate this model support-structure loading mechanism.

Introduction

THE National Transonic Facility (NTF) provides flight Reynolds number wind-tunnel testing capability using gaseous nitrogen as a test medium at cryogenic temperatures at pressures up to 8.8 atmospheres [1]. Cryogenic temperatures are obtained by spraying liquid nitrogen into the tunnel circuit. Although the maximum design dynamic pressure is 7000 psf, flight Reynolds numbers are achieved for most commercial aircraft models at dynamic pressures of about 3000 psf. Measurements of tunnel turbulence or unsteadiness, as typified by Fig. 1 from [2], indicate that the NTF is typical of slotted-wall transonic tunnels, with maximum-perturbation mean-square pressures of about 1% of dynamic pressure. Still, the very high dynamic load levels coupled with the unique structural design and construction requirements for cryogenic operations has brought forward the issue of model and structural vibrations.

The purpose of this paper is to present details of a novel aeroacoustic mechanism that plays a role in the model vibrations. Experience with model vibrations and measurements of tunnel unsteadiness are briefly summarized. Then the related topics of wind-tunnel resonance from the aeroelastic literature and Parker modes from the aeroacoustic literature are discussed. NTF measurements are then shown, indicating the presence of Parker mode interaction with strut dynamics during the occurrence of model vibrations under certain test conditions. Finally, an overview of structural modifications and tunnel vibration suppression made following the preparation of this paper is given.

Background

Young et al. [3] and Buerhle et a1. [4] gave details of model vibrations experienced in the NTF, focusing upon model yawing oscillations about the model support structure, shown in Fig. 2. The model, balance, and sting are connected to the model support structure, herein termed the strut, which consists of the moveable arc-sector quadrant (the forward half of the strut) and the aft aerodynamic body, termed the fixed fairing. The strut has a chord c of 9.2 ft, and the dimensions of the test section are 8.2 by 8.2 ft. Figure 3 shows the profile of the strut cross section and the wind-tunnel walls in the vicinity of the strut. The trailing edge of the fixed fairing has a 40 deg included angle. A slightly longer fairing would have allowed a smaller trailing-edge angle, but was precluded due to clearance for the plenum test-section-isolation gate-valve mechanism at the downstream plenum bulkhead. The walls diverge to allow area ruling of the strut thickness and aft of the trailing edge to allow the transition from the square test-section cross section to the conical diffuser section, with a diffuser-wall divergence half-angle of approximately 2.1 deg.

The arc sector is restrained laterally by four pairs of pucks or bearings, 2 at the top and 2 at the bottom. These pucks were originally designed for a 0.010 in. clearance [3]. It is noteworthy that the design specifications for the construction of the NTF contained very limited detail regarding dynamic loads. Loading conditions for sizing and design of the test-section and arc-sector components consisted only of pitch-plane loads. Dynamic loading in the yaw plane was not addressed. Adjustment of the pucks was troublesome and excessive clearance was shown to be detrimental for model vibrations. This led to a modified puck design, wherein positive contact between pucks and the arc sector is maintained using preloaded Belleville washers. Belleville washers consist of several concave-surfaced washers providing high stiffness under compression from the puck positioning bolts.

Vibration measurements performed on model balance/sting/strut combinations [4] have provided insight into the dynamics involved in the model vibrations. Frequencies vary with each particular combination tested and typically produce sting bending modes somewhat below 10 Hz, combination sting bending with model yawing about the balance somewhat above 10 Hz, and three modes involving the model support strut. For the combination studied in [3] these modes occurred at 19.2, 23.8, and 29.7 Hz. These strut modes result from the design requirements to accommodate thermal expansion/contraction of the tunnel structures. The fixed fairing is rigidly attached to the test-section backup structure at the top, but it is pinned at the bottom to restrain relative axial and lateral motions. This, plus the flexibility of the arc-sector restraints, gives rise to the vibration modes. The 29.7 Hz mode shape is indicated in Fig. 4 and is described as arc-sector/fixed-fairing rotation with model yaw on balance.

Young et al. [5] presented details of another type of model vibration in the NTF: rolling oscillations of a Boeing 767 model about the roll balance. This case did not involve other components of the model support structure and was shown to be induced by buffet onset of the model on the sting. Also documented was the elimination of the rolling oscillations when scaled replicas of the vortex generators installed on production aircraft were tested on the model. Particularly noteworthy was the sensitivity of the results to Reynolds number, emphasizing the importance of wind-tunnel tests at flight Reynolds number for such buffet onset testing.

Presented as Paper 0345 at the 35th Aerospace Sciences Meeting and Exhibit, Reno, NV, 6–10 January 1997; received 28 January 2007; accepted for publication 4 October 2008.

*Senior Research Engineer, Retired, Aeroelasticity Branch. Fellow AIAA.

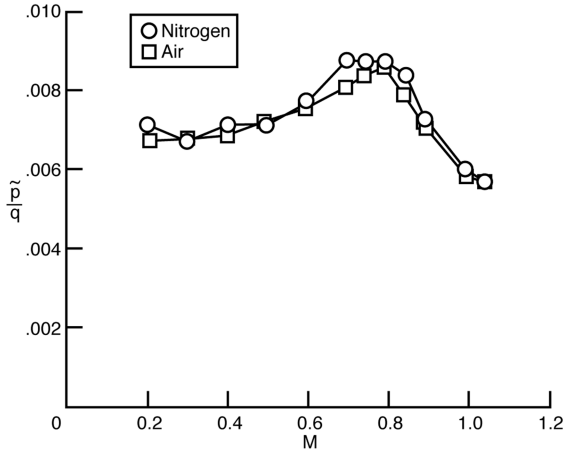

Fig. 1 Fluctuating pressure coefficient measured at test-section right-hand sidewall station 13; $Re = 10^6$ ft^{-1}; ambient temperature; air and nitrogen modes (from [2]).

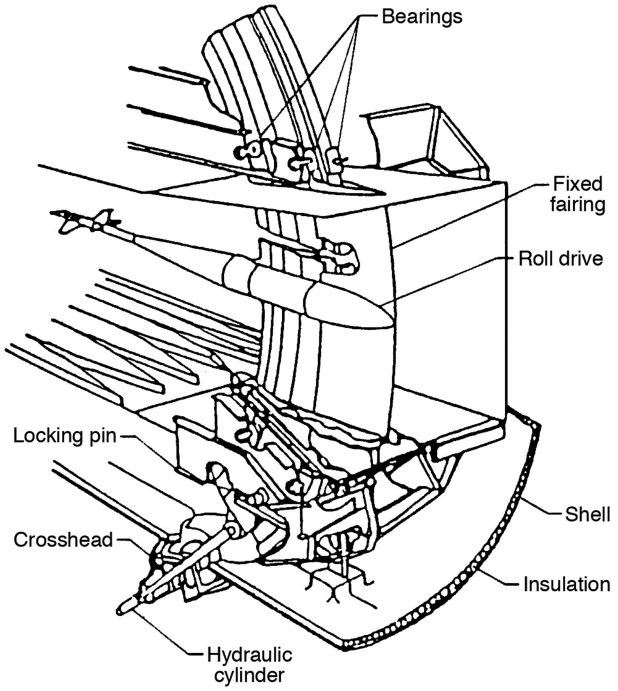

Fig. 2 NTF model support system (from [3]).

Igoe [2] made dynamic measurements of fluctuating pressure levels at 11 locations in the NTF circuit across the complete tunnel operating range, and many specific conclusions regarding the dynamic behavior of the tunnel are given. Most dynamic pressure spectra shown cover a wide frequency range (0–20 kHz) and do not focus on the 0–50 Hz range in which model vibrations occur and which is the focus of this study.

Following early evidence of model vibrations, two aeroelastic analyses were made of the NTF strut. Strganac [6] performed flutter analyses for Mach number $M = 0.5$ using doublet-lattice linear theory aerodynamics and found a tendency for a damping-dependent hump-mode instability within the operating envelope of the tunnel. Small levels of damping, always present in built-up structures, would eliminate such analytical instabilities, but the resulting lightly damped mode(s) are susceptible to disturbances and can produce high response levels. The wind-tunnel walls were not modeled in this study.

Whitlow et al. [7] performed similar aeroelastic analyses using the inviscid CAP-TSD (Computational Aeroelasticity Program–Transonic Small Disturbance) code. The analysis for several

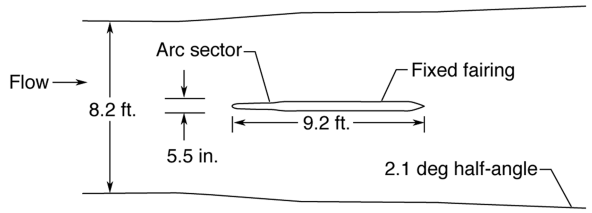

Fig. 3 Cross section along the tunnel centerline of NTF strut (arc sector plus fixed fairing) and tunnel sidewalls.

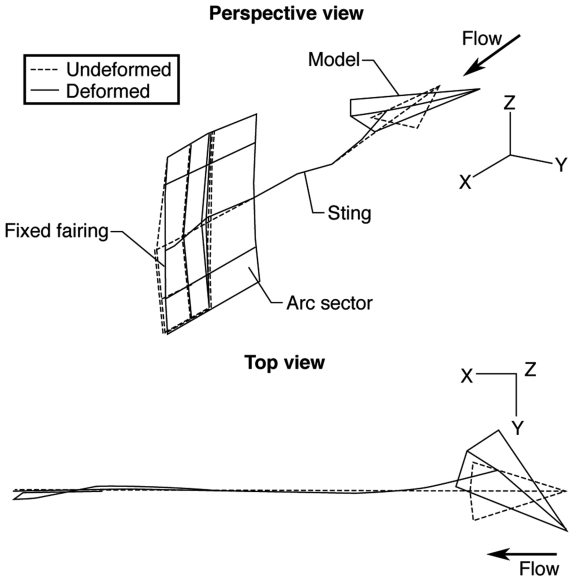

Fig. 4 Mode support strut, sting, balance, and model mode shape for 29.7 Hz vibration mode (from [4]).

subsonic Mach numbers again showed hump-mode instabilities for zero assumed damping. With the wind-tunnel walls modeled as parallel solid walls, the analysis showed the presence of an additional modal response, which was attributed to wall interference and which interacted with the structural modes involved in the hump-mode instabilities. The interaction was strongest for intermediate subsonic Mach numbers, leading to the observation that the mechanism might not be observed at higher-speed design conditions. The discussion of the additional mode in [7] identifies it as the wind-tunnel resonance frequency introduced by Runyan et al. [8]. It will be shown subsequently that this mode is instead a local acoustic mode studied extensively by Parker [9,10] and Parker and Stoneman [11] and termed the β mode.

Wind-Tunnel Resonance

Runyan et al. [8] studied the problem of an airfoil in a solid-wall subsonic wind tunnel undergoing forced pitching oscillations. The ratio of tunnel height to airfoil chord was 3.6:1. Measurements had shown that the lift and moment on the airfoil fell sharply at a frequency dependent upon Mach number. Subsonic integral-equation lifting-surface theory was developed for the airfoil between solid reflecting walls, and a numerical solution procedure was developed. It was noted that the kernel of the integral equation relating lifting pressure to the downwash boundary condition became infinite at frequencies

$$f_{\text{res}} = \frac{a_\infty \sqrt{1 - M^2}}{2h}(2n - 1), \qquad n = 1, 2, 3, \ldots \tag{1}$$

where a_∞ is the freestream sound speed and h is the tunnel height. Because the integrated product of the kernel and lifting pressure over the airfoil must equal the finite vertical velocity, the lifting pressure must become zero at these frequencies. The lowest frequency in this

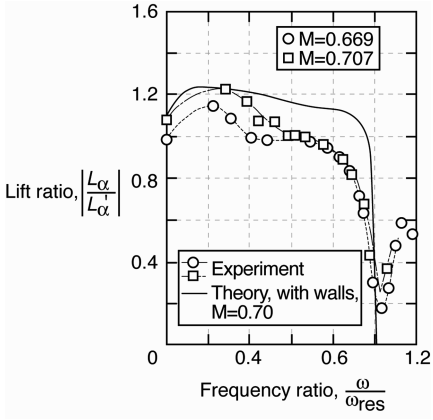

Fig. 5 Ratio of magnitude of lift in wind tunnel to lift in free air for a pitching airfoil with $h/c = 3.6$ (from [8]).

series for $n = 1$ has come to be termed the *tunnel resonance frequency* f_{res}. Calculations were accomplished for $f \leq f_{\text{res}}$, and a typical comparison with experiment is shown in Fig. 5 [8].

The lift ratio is the ratio of lift for the airfoil in the tunnel to the lift in free air. Most of the discussion in the ensuing aeroelastic literature of wind-tunnel wall interference in unsteady testing has focused mainly on the first $f_{\text{res}}(n = 1)$ eigenmode. It should be noted that this is an eigenmode of the empty wind tunnel, as the development of no lift can be seen as the result of the airfoil following the local vertical motion of the fluid oscillation in an undamped eigenmode. Thus, the fluid is unaware of the presence of the body and the same eigenmode obtained with the body removed.

Note that the experimental lift-ratio values in Fig. 5 do not go to zero at $f = f_{\text{res}}$ as does the theoretical value. This is due to an approximation made in [8], which led to the resonance condition [Eq. (1)]. From [8], "this approximation implies that the airfoil images, and particularly the closest image $n = 1$, are a sufficient distance from the airfoil that the actual distance $\sqrt{\xi^2 + \beta^2(nh)^2}$ may be replaced by the vertical distance βnh of the images above the airfoil."

This resonance frequency $f_{\text{res}}(n = 1)$ is the same as the ω_3 eigenmode of Lee [12], who studied resonant frequencies in open and closed three-dimensional empty wind tunnels using the finite element method. Mabey [13] further developed the resonance conditions for empty ventilated (slotted or porous) tunnels with plenum chambers. Resonance frequencies are shown to be below those of the closed tunnel for $M \leq 0.618$ and greater for $0.618 \leq M \leq 1.0$.

In this unsteady aerodynamic literature, the focus has been on undamped eigenmodes of the empty tunnel. In terms of the lift ratio shown in Fig. 5, this appears as an antiresonance. Attention is drawn to the damped resonance feature seen in Fig. 5 near $f \approx 0.2 f_{\text{res}}$, which has not been previously discussed. This is shown subsequently to be the β mode of Parker [9].

Parker Acoustic Modes

In a series of publications, Parker (e.g., [9–11]) studied acoustic resonances excited between cascades of parallel flat plates wherein the resonances are excited by vortex shedding from the blunted trailing edges. Parker [9] provided early calculations of the resonances and [11] is a summary article. Figure 6 from [9] indicates the typical configuration studied in a low-speed wind tunnel. Because of the repetitive geometry of the cascade, it was recognized that one cell of the cascade can be representative of a plate (or an airfoil or model support strut) between solid wind-tunnel walls. The acoustic modes observed by Parker are identified as local nonpropagating modes with frequencies below the empty-duct cutoff frequency. The four most prominent lower-frequency modes are termed the β, α, δ, and γ modes. Figure 7 from Kock [14] displays these calculated mode frequencies as a Parker mode diagram for $M = 0$ and a cascade with zero stagger angle. The notation (m, n),

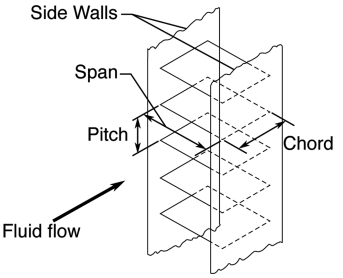

Fig. 6 Parker's experimental apparatus for investigating acoustic modes about parallel plates (from [9]).

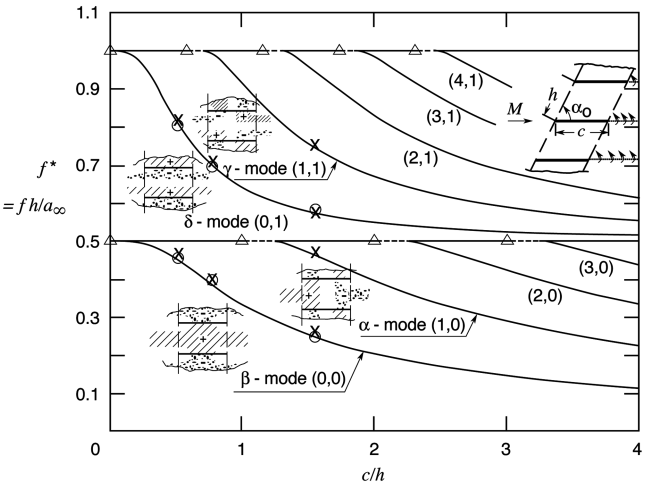

Fig. 7 Parker mode diagram for $M = 0$ and $\alpha_0 = \pi/2$; Parker experiment (○) and Parker computation (×) (from [14]).

commonly used for cavity modes, is employed to order the resonant modes. Here, m denotes the number of nodal lines of the pressure between the leading and trailing edges of the cascade and n denotes the number of nodal lines between two plates [14]. The shading in the inserts indicates the relative positive and negative pressure levels between plates for the four prominent modes. The circles in the figure represent Parker's experimental results and the crosses give Parker's numerical solutions (cf. Table I in [9]). The abscissa $f^* = fh/a_\infty = f/2f_{\text{res}}$ at $M = 0$ and it should be noted that as the chord c goes to zero the β-mode frequency approaches $f_* = 0.5$ and $f = f_{\text{res}}$. That is, the β-mode frequency approaches the empty tunnel wind-tunnel resonance-mode frequency of Runyan et al. [8] as the chord shrinks to zero.

All of these modes are acoustically nonpropagating and decay exponentially away from the airfoil. In the immediate vicinity of the plates, pressure fluctuations on the order of the dynamic pressure can be observed. Parker and Stoneman [11] commented that the resonant frequencies decrease with increasing Mach number in proportion to $(1 - M^2)^n$, where n depends on the ratio c/h and is in the range of $0.5 < n < 1.0$. Note that the Mach number dependence of Runyan et al.'s [8] wind-tunnel resonance mode, f_{res} is given by this relation with $n = 0.5$, which will be assumed in the following. Figure 5 in [14] demonstrates this trend for the β mode, also showing that the modal damping ratio increases from $\zeta = 0$ for $M = 0$ to $\zeta \approx 0.25$ for $M = 0.7$. For the NTF strut, $c/h \sim 9.2/8.2 = 1.12$ and $f_* \approx 0.32$ for the β mode. Thus, for the NTF strut,

$$f_\beta = 0.32(a_\infty/8.2)\sqrt{1 - M^2} \tag{2}$$

A good approximation for the speed of sound in both air and nitrogen is $a_\infty = 49\sqrt{T, {}^\circ\text{F} + 460}$ ft/s.

Parker [10] also investigated the effect of the β mode interacting with a flexible steel plate in a channel, a study that is interestingly similar to the NTF strut. By varying the channel width, the β-mode

frequency was able to be placed below, at, and above the fundamental plate-bending frequency. Very interesting details of the energy exchange between the airflow and the structural plate are discussed. Parker [11] summarized these results, recommending that the situation wherein f_β is slightly below the structural natural frequency is to be avoided because it produces the largest structural response levels.

Analysis

In this section, three efforts to analyze details of the aerodynamic and aeroelastic behavior of the strut are discussed. These efforts preceded the experimental measurements in the NTF to be discussed in the following sections.

First, results from the aeroelastic analysis of the strut by Whitlow et al. [7] using the inviscid CAP-TSD code are summarized in Figs. 8 and 9. Figure 8 gives perspective views of the finite element model vibration-mode shapes (developed from vibration testing of the strut) that were used in the analysis. The five modes used in the analysis [7] had natural vibration frequencies of 18.4, 24.98, 25.88, 42.59, and 25.19 Hz. There is very little displacement of the massive arc sector or of the fixed fairing at the ceiling to which it is cantilevered. The dominant motions occur over the lower portion of the fixed fairing, which acts much like a half-chord flap, and locally over the region in which the sting fairing loads are transmitted to the fixed fairing. Transient-response time histories of simulated strut motions were analyzed to extract frequencies and dampings. Figure 9 gives results for $M = 0.43$, 0.6, and 0.8 and for varying dynamic pressures. Calculations were made for the strut in free air (large computational grid) and for the strut between the NTF walls, modeled as solid, reflecting, parallel computational-grid boundaries. The results shown in Fig. 8 are with the walls modeled and show the root loci for increasing dynamic pressure. The loci of the five structural dynamic modes originate on the imaginary axis for zero pressure. Positive damping ratios ζ are stable and the results show hump-mode instabilities for $M = 0.43$ and 0.6. That is, small regions of negative damping are seen for limited ranges of dynamic pressure. Because the analysis is performed for zero assumed damping, realistic damping levels would be expected to provide stability. The free-air calculation, not shown, indicated that the strut was stable for all calculated pressure levels [7].

The figure also indicates that for the two lower Mach numbers, an additional mode, labeled q_R, was identified near 25–33 Hz. Now Eq. (2) predicts that the frequency of the β mode for $T = +120°$F and for $M = 0.43$ and 0.6 is $f_\beta = 41.5$ and 36.8 Hz, respectively. It is now evident that the q_r mode is the β mode interacting with the strut modes to produce the hump-mode instabilities shown in the figure.

The second analysis used a two-dimensional version of the inviscid CAP-TSD code to study the effects of strut and wall geometry modeling on the behavior of the strut unsteady airloads.

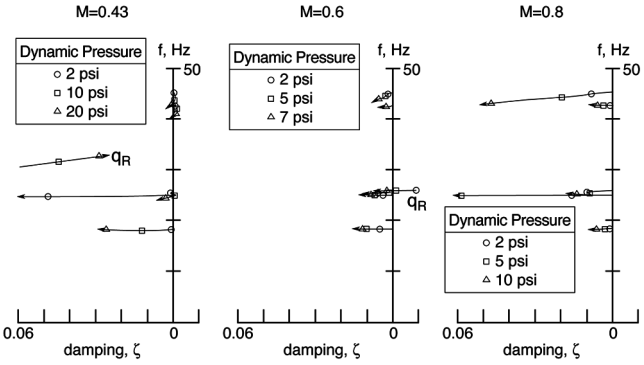

Fig. 9 Aeroelastic root loci of strut modes and β mode for varying Mach number and dynamic pressure calculated with CAP-TSD code (from [7]).

Simulated pulsed motions of the strut yawing about its midchord were computed and the resulting airloads were analyzed to obtain frequency-response functions. Figure 10 gives results for $M = 0.65$ for the yawing moment coefficient versus reduced frequency, $k = \omega c/2U_\infty$. In the free-air solution (Fig. 10a), no resonances are seen, whereas pronounced resonances are seen for the three cases with walls modeled. For the cases with parallel walls (Figs. 9b and 9c), solid-wall boundary conditions were used at the left- and right-hand-side computational-grid boundaries. For the case with the NTF diverging walls (Fig. 9d), the walls were simulated as two additional thin, static, lifting surfaces extending well upstream and downstream of the simulated NTF strut.

In Fig. 10b, the β mode is seen at $k = 0.85$, which corresponds to $f_\beta = 33.8$ Hz for the NTF strut. Also seen is the antiresonance f_{res} for which the amplitude of the airloads drops nearly to zero. Finally, two additional prominent resonances at higher frequencies are noted. The first of these, labeled f_η here, occurs at approximately $5f_\beta$ and would appear to be a higher-order Parker mode than those shown in Fig. 7.

Figure 10c indicates that these features are unchanged with the introduction of the strut geometry and the transonic small disturbance (TSD) equation. On the other hand, introducing the wall divergence (Fig. 10d) affects the three features discussed previously: the f_β and f_{res} features are no longer seen and the f_η resonance is much enhanced. This is indicative of selective tuning of these local acoustic modes through small changes of body and wall boundary geometries. Calculations, not shown, with a viscous version of the 2-D CAP-TSD code [15,16] using an interactive boundary-layer method, show dominant self-excited β-mode activity for the conditions of Fig. 10d. This is due to the slight, though critical, change to the effective strut geometry introduced by the boundary-layer displacement thickness.

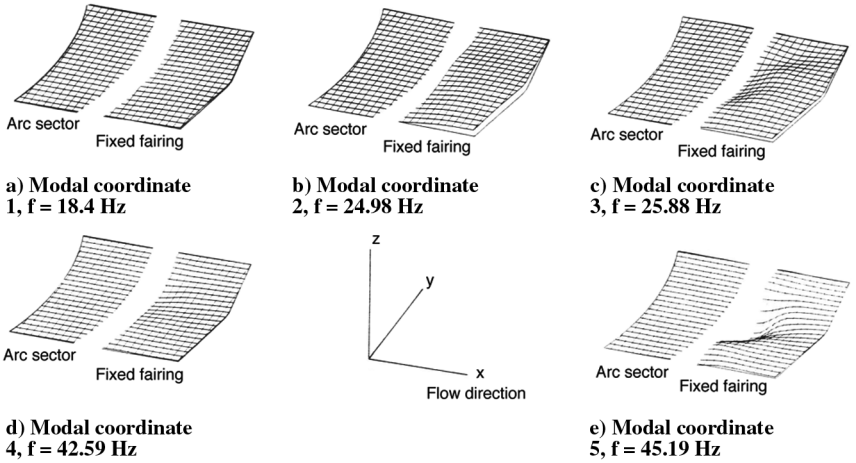

Fig. 8 Perspective view of arc-sector and fixed-fairing finite element model vibration-mode shapes of the first five modes used in flutter analysis (from [7]).

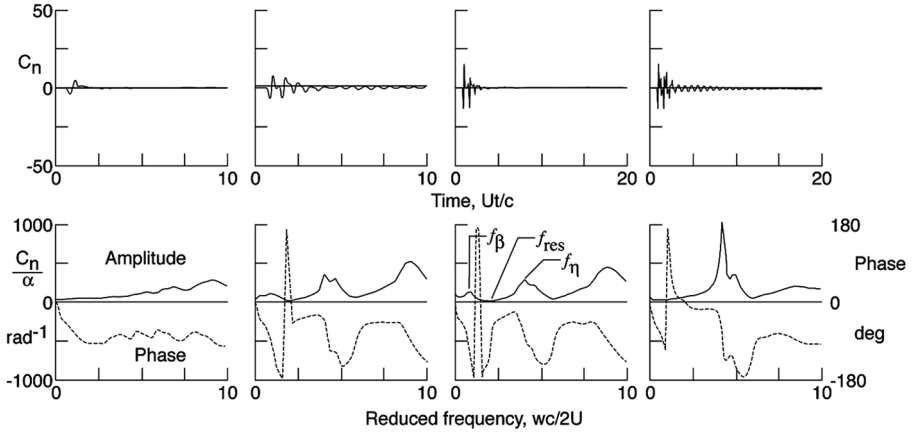

a) Linear equation, flat-plate geometry, free-air solution | **b) Linear equation, flat-plate geometry, parallel walls** | **c) TSD equation, strut geometry, parallel walls** | **d) TSD equation, strut geometry, NTF diverging walls**

Fig. 10 Frequency responses for strut yawing moment due to strut yawing calculated with CAP-TSD code; $M = 0.65$ and ambient temperature.

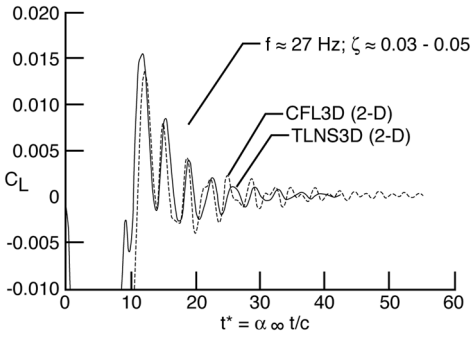

Fig. 11 Strut lift-coefficient transient responses calculated with Reynolds-averaged Navier–Stokes codes: $M = 0.65$, ambient temperature.

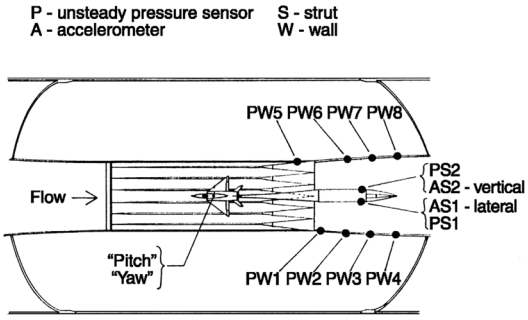

Fig. 12 Instrumentation for the present investigation.

The final analysis to be discussed is for the geometry boundary conditions of Fig. 10d, but with higher-order computational codes. Calculations were made with two Reynolds-averaged Navier–Stokes (RANS) codes to study the fluid dynamic behavior of the flow about the strut. These codes are described in [17], in which their use in calculating transonic shock-induced oscillations about airfoils is shown (capability of computing the same shock-induced oscillations about airfoils is shown in [15] for the viscous CAP-TSD code). Figure 11 gives transient responses calculated with the CFL3D and TLNS3D codes. Perturbations were introduced and the yawing moment coefficient responses for $M = 0.65$ and $t^* = a_\infty t/c$ show damped β-mode response at 27 Hz with $\zeta \sim 0.03$–0.05. These calculations and the preceding viscous TSD calculations indicate a marked sensitivity to the detailed viscous flow at the strut trailing edge, which has a 40 deg included angle closure. Both types of flow modeling indicated a small region of flow separation at the trailing edge, on the order of several percent chord length. However, the viscous TSD calculations showed large self-excited β-mode flow oscillations, whereas the RANS results are damped.

Instrumentation

The model installed in the tunnel was the high-speed-research model described in [3]. Data were recorded for playback analysis on a 28-channel analog tape recorder. Spectral analysis was accomplished with a Spectral Dynamics analyzer with 4-channel input capability. Frequency spectra were generally analyzed for a 0–100 Hz bandwidth, and analog low-pass prefilters were used. For these measurements, data were recorded from the time of the start of the tunnel drive fan until the tunnel had achieved test conditions at $M = 0.9$, generally about 10–30 min. The results shown subsequently were obtained with 100 spectral averages and, due to the changing tunnel conditions, some smearing of spectral features should be expected. Instrumentation installed to study the behavior of the strut is indicated in Fig. 12. Eight unsteady pressure transducers were placed on the tunnel sidewalls along the tunnel centerline at approximately 0, 33, 67, and 100% chord. On the far sidewall, the leading sensor was placed approximately 33% chord ahead of the strut leading edge. Two additional unsteady pressure sensors were installed on opposite sides of the fixed fairing, near the aft end of the flat section of the fairing. At the same locations, two accelerometers were placed to measure the strut (fairing) lateral and vertical accelerations. Finally, two strain-gauge measurements were obtained from the model balance, one indicative of pitching moment and the other indicative of yawing moment. Because of concern over tunnel data system integrity, these single strain-gauge measurements are uncalibrated and only relative amplitudes can be given. The measurements shown subsequently are from this yaw signal, the PW7 sidewall pressure sensor, and the AS1 lateral strut accelerometer.

Results

Frequency spectra from the three sensors described previously are shown in Fig. 13 for $T = +120$ and -250°F and for $M = 0.2$, 0.4, 0.6, and 0.9. This results in dynamic pressures in the test section of 965 psf for the ambient temperature and 2680 psf for the cryogenic temperature at $M = 0.9$. Attention is drawn to the behavior of the spectra in the 20–40 Hz frequency range, as it is this range in which the largest model vibrations are observed. The yaw spectra typically contain several resonance peaks below 20 Hz, which are associated with sting and model/balance/sting/strut dynamics. This model/balance/sting combination also has a resonance peak in the range of 25–28 Hz, which is in close proximity to the resonance usually seen in the strut lateral acceleration AS1 spectra.

The sidewall pressure spectra from the PW7 sensor show spectral features below 20 Hz, which maintain the same general shape for the differing conditions, rising in amplitude with increasing Mach

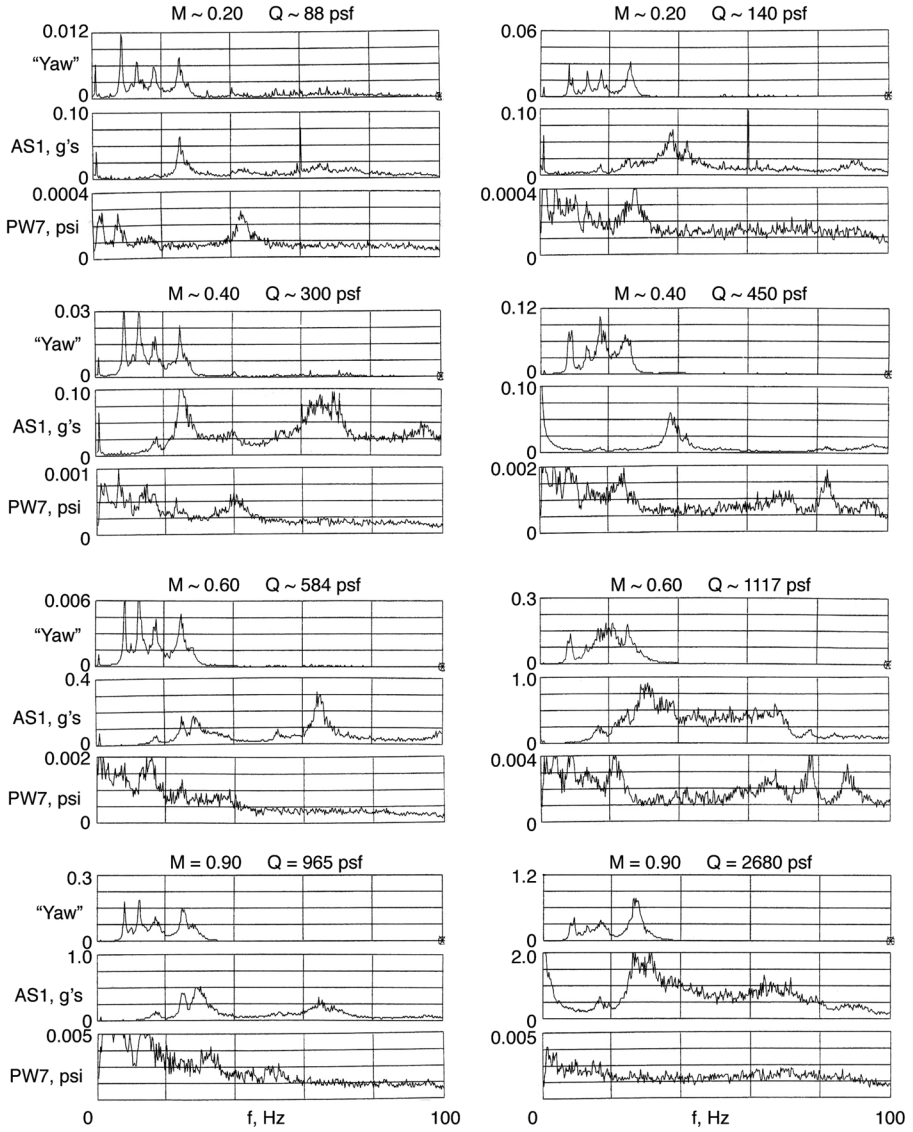

Fig. 13 Frequency spectra from high-speed-research model test.

number and dynamic pressure. The key features to be noted are the spectral peaks seen in the PW7 spectra near 44 Hz for $T = +120°\text{F}$ and $M = 0.2$ and near 27 Hz for $T = -250°\text{F}$ and $M = 0.2$. These resonances decrease in frequency with increasing Mach number for both temperatures, becoming difficult to distinguish for the higher Mach numbers. This resonance is that of the Parker β mode as can be seen from the agreement of these measured frequencies with those predicted by Eq. (2) in Table 1. The agreement is quite good for the lower Mach numbers, at which the mode is distinct. The difficulty in discerning the mode at the higher Mach numbers is consistent with the increased damping at higher Mach numbers discussed previously. The other pressure sensors, including the two on the strut, show spectral features similar to those shown in Fig. 13.

Table 1 Frequency of β mode versus Mach number and temperature for the NTF model support strut

	$T = +120°\text{F}$		$T = -250°\text{F}$	
	f, Hz		f, Hz	
M	Equation (2)	Exp.	Equation (2)	Exp.
0.0	46.0	——	27.7	——
0.2	45.0	43.0	27.2	28.0
0.6	36.8	~40	22.2	23.0
0.8	27.6	——	16.6	~21
0.9	20.1	~33	12.1	——

The relative amplitude of the yaw spectral peak at 25–28 Hz is indicative of the amplitude of model vibrations. Figure 14 summarizes this feature for the high-speed-research model. Data from test runs at three additional temperatures are given. The test condition for each run was $M = 0.9$, and differing tunnel static pressures lead to differing maximum dynamic pressures, which in turn is indicative of the maximum power in the flow within the tunnel. It should be expected that the amplitude of model vibration would increase with increasing dynamic pressure, assuming broadband nonresonant turbulence as a loading mechanism. This generally rising level of yaw response with increasing dynamic pressure is seen in Fig. 14 and, in addition, a local maximum response is observed, most pronounced for $T = -180°\text{F}$ and $M = 0.7$. Noting that the frequency of the β-mode resonance sweeps through this 25–28 Hz range of the model yaw response, it is evident that this is the mechanism producing the local maximum response motions. It is also apparent that this is not the mechanism responsible for the larger response shown at the highest dynamic pressures. Still, much testing is performed at lower power conditions, and understanding of this loading mechanism might lead to better tunnel performance at those conditions in which it can be present.

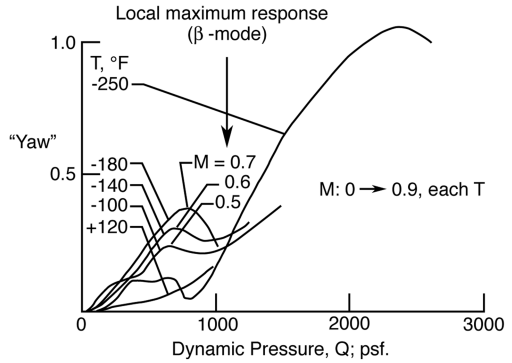

Fig. 14 Peak amplitude of Yaw spectrum for $f \sim 25$–28 Hz for five temperature-static pressure runs: Mach number varies from 0 to 0.90 for each run.

In summary, the presence of the β mode is not sufficient in itself to explain observed model vibrations for the highest power conditions. As the analyses discussed previously indicated, for these conditions, the frequency of the β mode is well below the dominant-strut modal frequency, and other excitation mechanisms are necessary to complete the understanding of the situation.

Conclusions

Investigations into the causes of model vibrations in the National Transonic Facility have been described. The relationship between wind-tunnel resonance encountered in the unsteady aerodynamic literature and local aeroacoustic features known as Parker modes is explained. The lowest frequency of these modes, the β mode, is shown to interact with structural dynamic modes of the NTF model support structure in aeroelastic analyses. Measurements from the NTF demonstrate the presence of the β mode and indicate that a portion of the vibration response of the model support structure and the attached model can be attributed to this mechanism.

Following the completion of the study described in this paper, a concentrated effort was undertaken to suppress the vibrations of the model support-strut structure [18]. A greatly expanded data acquisition operation led to a more complete understanding of the dynamic loads operating upon the tunnel structures and their dynamic response characteristics. Solutions chosen for implementation were to increase the support-structure stiffness and to change several of the support-structure boundary conditions. Stiffness was added with shear plates, bulkheads, and brackets mounted above and below the tunnel-circuit ceiling and floor walls, respectively. Boundary conditions were modified with wedges between the fixed fairing and the floor to further restrain lateral motions and with additional arc-sector bearings that were actively controlled to suppress vibrations. These efforts led to a 90% reduction in vibrations of the model support strut [18] and a small reduction in model vibrations (which are dominated by model/balance/sting characteristics).

Acknowledgments

The author would like to thank Christopher Rumsey, Mark Sanetrik, Robert Biedron, Duane Melson, and Edward Parlette of NASA Langley Research Center's Computational Aerodynamics Branch for providing the Reynolds-averaged Navier–Stokes code calculations shown in Fig. 11.

References

[1] Bruce, W. E., Jr., and Gloss, B. B., "The U. S. National Transonic Facility," *Special Course on Advances in Cryogenic Wind Tunnel Technology*, AGARD Rept. AGARD-R-774, Neuilly-sur-Seine, France, Nov. 1989, Paper 3.

[2] Igoe, W. B., "Analysis of Fluctuating Static Pressure Measurements in the National Transonic Facility," NASA TP-3475, Mar. 1996.

[3] Young, C., Popernack, T., and Gloss, B., "National Transonic Facility Model and Model Support Vibration Problems," AIAA Paper 90-1416, 1990.

[4] Buehrle, R. D., Young, C. P., Jr., Balakrishna, S., and Kilgore, W. A., "Experimental Study of Dynamic Interaction Between Model Support Structure and a High Speed Research Model in the National Transonic Facility," AIAA Paper 94-1623, 1994.

[5] Young, C. P., Jr., Hergert, D. W., Butler, T. W., and Herring, F. M., "Buffet Test in the National Transonic Facility," AIAA Paper 92-4032, 1992.

[6] Strganac, T. W., "A Study of Aeroelastic Stability for the Model Support System of the National Transonic Facility," AIAA Paper 88-2033, 1988.

[7] Whitlow, W., Jr., Bennett, R. M., and Strganac, T. W., "Analysis of Vibrations of the National Transonic Facility Model Support System Using a 3-D Aeroelastic Code," AIAA Paper 89-2207, 1989.

[8] Runyan, H. L., Woolston, D. S., and Rainey, A. G., "Theoretical and Experimental Investigation of the Effect of Tunnel Walls on the Forces on an Oscillating Airfoil in Two-Dimensional Subsonic Compressible Flow," NACA Rept. 1262, 1956.

[9] Parker, R., "Resonance Effects in Wake Shedding from Parallel Plates: Calculation of Resonant Frequencies," *Journal of Sound and Vibration*, Vol. 5, No. 2, 1967, pp. 330–343. doi:10.1016/0022-460X(67)90113-7

[10] Parker, R., "The Effect of the Acoustic Properties of the Environment on Vibration of a Flat Plate Subject to Direct Excitation and to Excitation by Vortex Shedding in an Airstream," *Journal of Sound and Vibration*, Vol. 20, No. 1, 1972, pp. 93–112. doi:10.1016/0022-460X(72)90765-1

[11] Parker, R., and Stoneman, S. A. T., "The Excitations and Consequences of Acoustic Resonances in Enclosed Fluid Flow Around Solid Bodies," *Proceedings of the Institution of Mechanical Engineers Part C, Mechanical Engineering Science*, Vol. 203, No. 13, 1989, pp. 9–19. doi:10.1243/PIME_PROC_1989_203_081_02

[12] Lee, I., "Resonance Prediction for Closed and Open Wind Tunnels by the Finite-Element Method," *AIAA Journal*, Vol. 27, No. 4, Apr. 1989, pp. 391–398. doi:10.2514/3.10125

[13] Mabey, D. G., "The Resonance Frequencies of Ventilated Wind Tunnels," Royal Aircraft Establishment TR 78038, Farnborough, England, U.K., 1978.

[14] Kock, W., "Resonant Acoustic Frequencies of Flat Plate Cascades," *Journal of Sound and Vibration*, Vol. 88, No. 2, 1983, pp. 233–242. doi:10.1016/0022-460X(83)90639-9

[15] Edwards, J. W., "Transonic Shock Oscillations Calculated with a New Interactive Boundary Layer Coupling Method," AIAA Paper 93-0777, 1993.

[16] Edwards, J. W., "Transonic Shock Oscillations and Wing Flutter Calculated with an Interactive Boundary Layer Coupling Method," NASA TM 110284, Aug. 1996.

[17] Rumsey, C. L., Sanetrik, M. D., Biedron, R. T., Melson, N. D., and Parlette, E. B., "Efficiency and Accuracy of Time-Accurate Turbulent Navier-Stokes Computations," AIAA Paper 95-1835, 1995.

[18] Kilgore, W. A., Balakrishna, S., and Butler, D. H., "Reduction of Tunnel Dynamics at the National Transonic Facility," 39th AIAA Aerospace Sciences Meeting and Exhibit, AIAA Paper 2001-1162, Reno, NV, Jan. 2001.